High defense system expression broadens protection range at the cost of increased autoimmunity

Nitzan Aframian[1×], Shira Omer Bendori[1×], Tal Hen[1], Polina Guler[1], Avigdor Eldar[1]*

1. Shmunis School of Biomedicine and Cancer Research, Faculty of Life Sciences, Tel-Aviv University, Tel-Aviv, 69978, Israel.

[×]equal contribution

*Corresponding author

Abstract

The evolutionary arms race between bacteria and their phage viruses has given rise to elaborate anti-phage defense mechanisms. Major advances have been made in revealing the molecular details underlying diverse defense systems, but general principles and constraints are largely unkown. Defense systems are often tested against a diverse set of phages, revealing widely varying protection ranges. While these disparities are usually attributed to differences in mechanism, here we show that increasing expression of defense systems can greatly enhance their protection range. This holds true for disparate mechanisms, and is achieved by circumventing phage strategies for overcoming bacterial defense. However, increased defense system expression comes with a heavy cost of autoimmunity. Therefore, the expression level of defense systems controls a tradeoff between protection range on the one hand and autoimmunity on the other. We discuss how this tradeoff may drive the regulation of defense systems expression and the acquisition of multiple systems within the same genome.

Introduction

Every known life form is plagued by viruses, and bacteria are no different. Accordingly, it is increasingly appreciated that bacteria employ a diverse set defense system against their viruses, called phages[1–3]. A basic step often performed in the characterization of newly found systems, is to outline their protection range by testing their ability to defend against a variety of phages. While some systems have been shown to protect bacteria against a broad set of phages[2,4–6], others seem to confer a far narrower protection range, defending only against particular phages[7,8].

Great progress has been made in understanding how the underlying molecular mechanisms of defense affect the protection range afforded by different systems. For instance, different homologs of the CapRel defense system confer protection against different phages[9]. It has been shown that this may be explained by phage-specific variations in particular residues of the major capsid protein, which acts as the trigger of this system. Accordingly, residues of CapRel thought to directly bind the major capsid protein are highly variable, suggesting 'Red Queen' evolutionary dynamics[9]. In contrast, different homologs of the Avs system were shown to confer extremely broad protection range due to recognition of widely conserved structural patterns of phage components that share very low sequence identity[6].While mechanisms of defense are rapidly being elucidated, other factors affecting the protection range of different systems remain largely unexplored. Anecdotally, mechanism-independent factors such as temperature[7,10] and expression level[11] have been found to affect the protection range of different defense systems. However, systematic investigation of such factors, particularly factors that bacteria can control, is lacking.

Here, we explore the consequences of defense system expression levels. We find that increasing the expression of diverse defense systems can substantially enhance their protection range. Our results agree with the hypothesis that this is a consequence of overcoming different phage strategies to counter defense. However, we also find that increased defense system expression comes at an increased cost to bacteria. We show that this cost does not result from the energetic burden of expression but is rather due to the activity of defense systems, and is therefore a form of autoimmunity. The tradeoff between protection range and expression-associated cost may provide a potential explanation for the low native expression of different systems, density-dependent expression regulation[12–14], and the acquisition of multiple specialized defense systems within the same genome[1].

Results

Increased expression of the *spbK* defense system extends its protection range

To test the hypothesis that increased defense system expression leads to increased protection range (Fig. 1A), we began by focusing on the newly discovered defense system, SpbK. SPbK is a single-gene abortive infection defense system that naturally resides on the ICE*bs*1integrative and conjugative element, native to lab strains of *Bacillus subtilis*, which also host the SPβ prophage[8]. This system was shown to confer protection against phage SPβ by recognizing the YonE phage protein, and initiating growth arrest in response[8]. At native *spbK* expression levels, no defense was found against several other phages tested, indicating a relatively narrow range of protection. To test the effect of *spbK* expression levels, we constructed a strain with *spbK* under its native promoter (*spbK*^{wt}), and a strain with *spbK* under an IPTG-inducible promoter (*spbK*^{ind}). To focus specifically on the effect of *spbK* both these strains harbor *spbK* alone without the full ICE*bs*1. First, we used RT-PCR to better understand the relative

74 expression levels of native and induced *spbK*. We found expression of *spbK*^{wt} to be
75 relatively low, corresponding to induction with less than 5 µM IPTG (Figure S1A). This
76 is comparable to *spbK* expression levels when residing within ICE*bs*1.

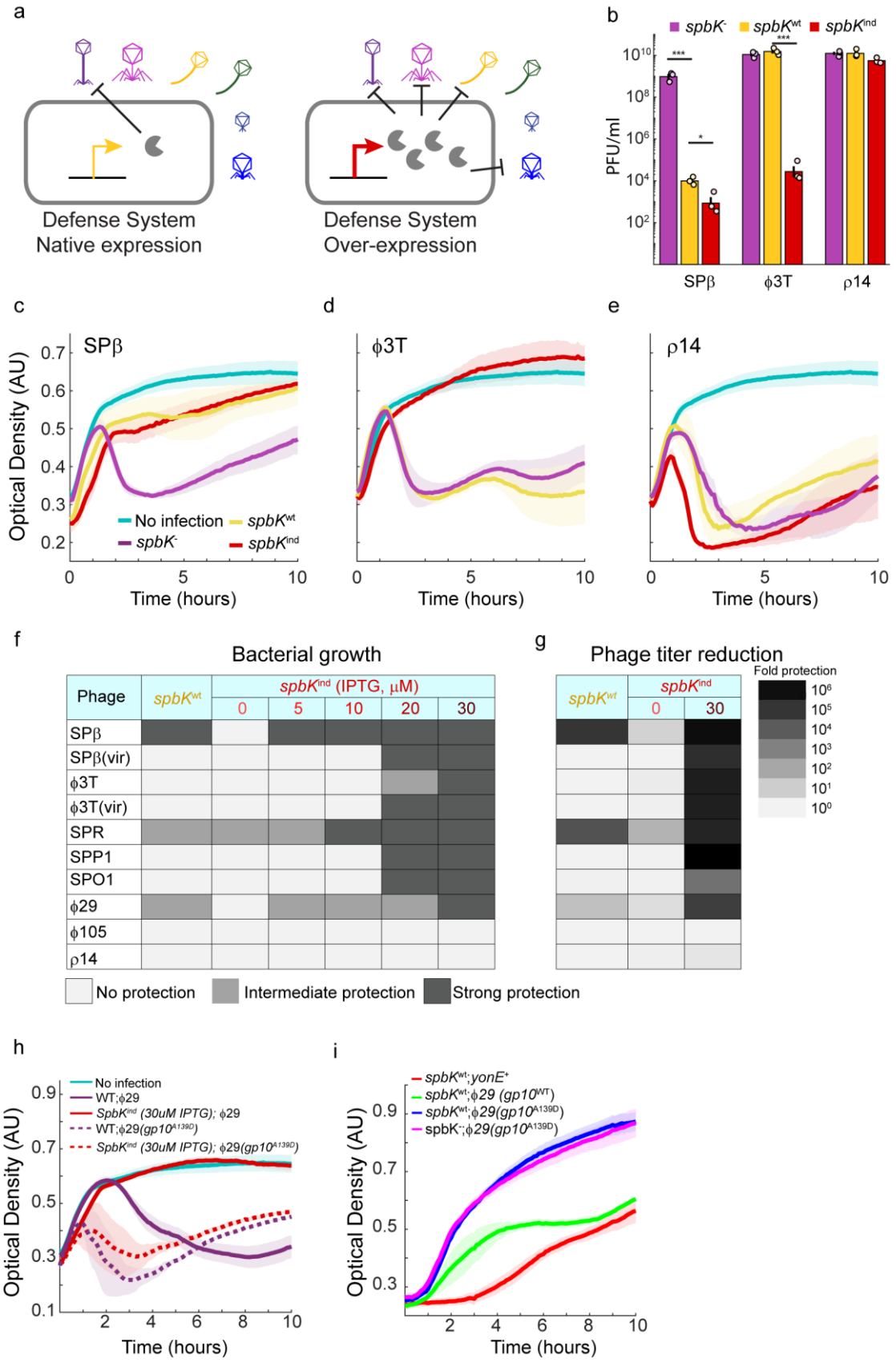

77

Figure 1: Over expression of the *spbK* defense system extends its protection range. (a) Illustration of the extension hypothesis. (b-e) PFU (b) and growth curves (d-e) after infection of phages Spβ (b,c), ϕ3T (b,d) and ρ14 (b,e). Phages infected either a defenseless background strain (*spbK*$^{-}$, purple), a strain encoding for *spbK* under its native promoter (*spbK*^{wt} strain, yellow) or a strain overexpressing SpbK (*spbK*^{ind} strain with 30µM IPTG, dark red). In (b) the geometric means and error bars represent the s.e.m. of the log are shown. Empty circles represent n = 3 biological replicates; * marks p<0.05, *** marks p<0.0005. In (d-e). mean OD of n=3 biological replicates and and s.e.m. (lighter shade) are shown. Growth of non-infected cells is also shown in cyan. (f,g) Level of protection inferred from (f) growth curve and (g) PFU for 10 designated phages infecting either *spbK*^{wt} or *spbK*^{ind} with different levels of IPTG (See also Figure S2and S3). Color code for protection levels is explained in the legends. (h) Comparison of infection curves of phages ϕ29 (solid line) and its escaper mutant ϕ29(gp10^{A139D}) (dashed line) upon infection of wild-type (purple) and *spbK*^{ind} (30µM IPTG, deep red) strains. (i) Growth curves of cells coexpressing the natively expressed *spbK* gene and either of three xylose-induced portal proteins; *yonE* (red) from phage SPβ, *gp10* from phage ϕ29 (green) or *gp10*^{A139D} escaper mutation (blue). The latter strain is also shown with no *spbK* gene coexpression as a control (magenta).

Next, we tested the protection range of *spbK* at different expression levels against a diverse set of phages by tracking bacterial growth during infection as well as phage propagation 2 hrs post infection (Methods; Fig 1B-G, Figure S2, S3). To this end we used a diverse set of 10 phages and phage mutants that differ in their lifestyle and belong to different morphological families. All infection experiments were performed on bacteria grown to mid-log phase in liquid lysogeny broth (LB) at a multiplicity of infection (MOI) of 0.1. In terms of growth curves, we differentiated no reduction in OD (strong protection), and a diminished or delayed reduction in OD (weak protection) (Fig. 1C-F; Figure S3). At native expression levels, we found that *spbK* strongly protects against phages SPβ and SPR with observed ~5 and ~4 orders of magnitude reduction in phage titer respectively, and no inhibition of bacterial growth (Fig 1B-G). Apart from these phages, which both belong to the SPβ-like family[15–17], natively expressed *spbK* offered only weak protection against phage ϕ29 (a 10-fold reduction in phage production that did not prevent bacterial population collapse). Increasing expression led to protection against some additional phages but not others. For example, overexpression of *spbK* conferred potent protection against phage ϕ3T – phage propagation was reduced by ~5 orders of magnitude, and bacterial growth curves during infection did not observably deviate from infection-free growth curves (Fig. 1B, D; Figure S2, S3). In contrast, phage ϕ105 remained unaffected even when *spbK* was overexpressed – no discernable defensive effect of native nor overexpressed *spbK* was found in terms of bacterial growth or phage propagation (Fig. 1B, E; Figure S2, S3).

Overall, protection range dramatically increased with increased *spbK* expression – at 30 µM IPTG, which corresponds to a ~20-fold increase compared to native expression (Figure S1A), SpbK provided potent protection against all phages tested, with the exclusion of ϕ105 and ρ14 which both belong to the ϕ105-like family (Fig. 1F, G). In terms of growth curves, we found that some offered only weak protection, while others allowed for completely uninterrupted population growth. We also found that when *spbK* was overexpressed, phage propagation was reduced by more than 3 orders

of magnitude for each of these 8 phages. Notably, overexpressed, but not natively expressed *spbK*, could not protect against a virulent mutant of SPβ deleted in its master repressor[18,19]. This difference between WT SPβ and its virulent mutant may stem from a more rapid infection cycle of the mutant[20].

SPbK can be triggered by divergent portal proteins

Interestingly, SPP1, ϕ29 and SPO1 are among the phages strongly inhibited by overexpressed *spbK*, but they do not code for a protein with high sequence identity to the SPbK-triggering YonE protein of SPβ. YonE was previously proposed to function as a portal protein based on homology search and its vicinity to a putative terminase[8]. Portal proteins of diverse phages tend to have a similar structure despite little sequence identity, and it was recently discovered that some Avs systems can recognize highly divergent portal proteins [6]. We therefore hypothesized that SPbK can similarly recognize diverse portal proteins, even when those share little sequence identity.

To test this, we focused on the portal protein of phage ϕ29, Gp10, which has been characterized structurally and functionally [21–23], and shares a low (12.5%) amino acid sequence identity with YonE. We infected bacteria expressing high levels of SPbK that are sufficient to hinder ϕ29 propagation in liquid LB, and performed plaque assay on defenseless bacteria after 2 hrs. We then tested phage isolates from several plaques for their ability to infect bacteria that express high levels of *spbK* by tracking growth curves, confirming 8 escaper mutants (Fig. 1H). We sequenced *gp10* from every escaper mutant and found that they all harbored the same point missense A139D mutation, which is located at an exposed residue that faces outwards from the portal ring, and is predicted to be highly variable (methods)[23,24]. The fact that all isolates harbored the same mutation may have resulted from a single mutant taking over the population during infection in the well-mixed liquid culture, or from multiple parallel mutations.

Notably, escaper mutants caused an earlier population collapse when infecting the *spbK*$^-$, defenseless, stain compared to their ancestor, followed by population recovery (Fig. 1H). The ability of these mutants to escape defense may result from altered infection dynamics that may not directly reflect on the role of Gp10 as a trigger for SpbK. To validate that SpbK can be triggered by the portal Gp10 protein of ϕ29, we co-expressed it in bacteria along with natively expressed *spbK* (Fig. 1I). Highly expressed *gp10* resulted in growth inhibition in the presence of SpbK, but not in its absence. Though substantial, the toxicity exhibited by co-expression of *spbK* and *gp10* was weaker than that of *spbK* and *yonE*. This is in line with the observation that SpbK strongly protects against ϕ29 only when overexpressed. In contrast, co-expression of *spbK* along with the mutant *gp10* found in ϕ29 escapers did not result in growth inhibition, pointing to a reduced ability to trigger SpbK. Overall, these results indicate that during phage infection SpbK can potentially be triggered by diverse portal proteins to provide potent defense. This potential is realized at high levels of expression, facilitating a broadening of protection range.

164 **Extension of protection range upon overexpression is found in three additional**
165 **defense systems; Lamassu, Gabija and Septu**

166 We wondered if this pattern of protection range increasing along with expression
167 could be generalized to other defense systems. To test this, we examined three
168 additional defense systems from different *Bacillus* species – Gabija, Lamassu, and
169 Septu[2], each of which was cloned under its native promoter or under an inducible
170 promoter (either IPTG or xylose induction) into *Bacillus subtilis*. We tested the
171 protection capability of each of these systems against the same set of 10 phages and
172 lytic phage mutants. We found that overexpression increased protection range for all
173 systems as measured by growth curves, attesting to the generality of the relationship
174 between expression level and protection range (Fig 2A, Figure S4-S6).

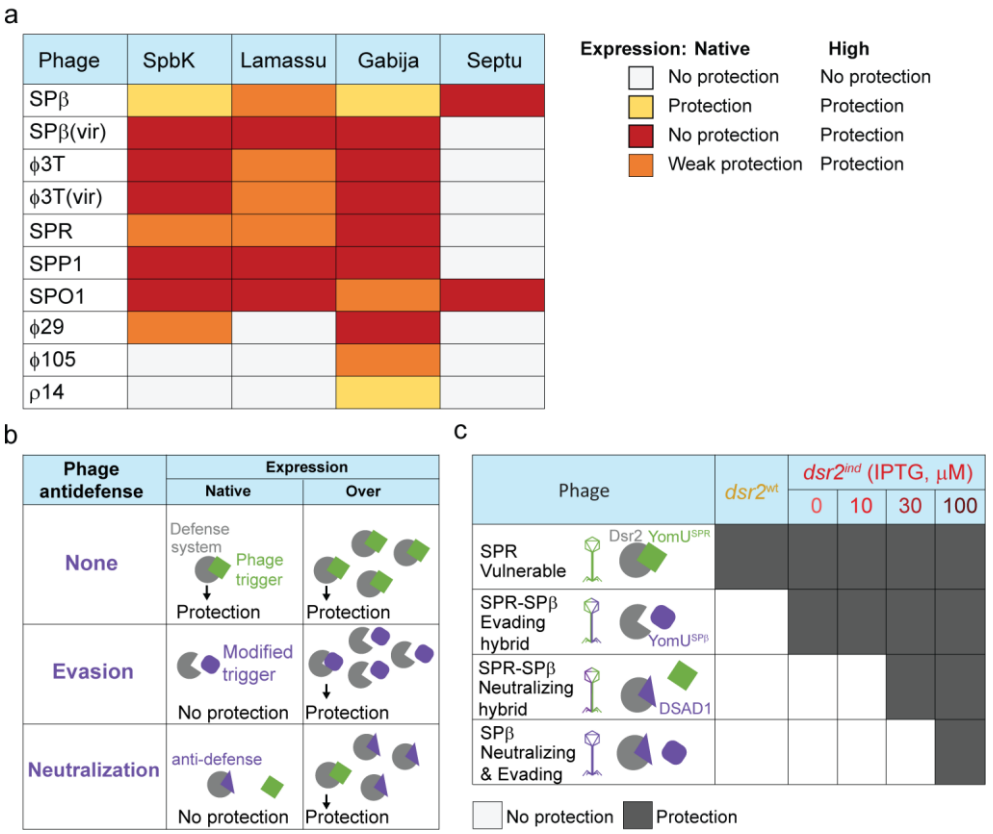

175

176 Figure 2: Extended protection range upon overexpression occurs in multiple defense systems
177 and depends on overcoming different counter-defense strategies. (a) A table summarizing
178 protection afforded by defense systems as native expression and when overexpressed, as
179 inferred by growth curves (See also Figure S3-S6). Color code for protection levels is explained
180 in the legends. (b) Illustration of a hypothesis for the mechanism underlying extended
181 expression range. Increased protection overwhelms counter defense strategies of evasion and
182 neutralization. (c) Table summarizing protection afforded by the DSR2 system at different
183 expression levels against phages SPR, SPβ, and their hybrids. Results are based on efficiency
184 of plating (EOP; See also Figure S7).

185 **Overexpression of the DSR2 defense system allows it to overcome different**
186 **strategies employed by phages to circumvent defense**

187 Next, we wanted to examine the underlying cause for the observed increase in
188 protection range. We hypothesized that increased expression may overwhelm
189 different strategies phages employ to circumvent bacterial defense (Fig. 2B). From a
190 broad perspective, two strategies phages employ to overcome bacterial defense are
191 evasion and neutralization. Evasion may be achieved, for example, by changing the
192 phage component that acts as the trigger of defense[9,25]. Alternatively, phages can
193 actively neutralize bacterial defense by encoding an anti-defense mechanism[11,26,27].
194 We reasoned that expression levels of defense systems may be crucial for the success
195 of both these general strategies. For the evasion strategy, a lower affinity to the trigger
196 of defense may be compensated for by a higher concentration of the defense system
197 itself, potentially allowing bacteria to maintain rapid phage detection and effective
198 defense activation. For the neuralization strategy, defense systems may be expressed
199 at a level which overwhelms phage-encoded antidefense mechanisms.

200 Initial support for this mechanistic explanation can be found in the pattern of Gabija
201 defense against phage ϕ3T[27]. Natively expressed Gabija defends against phage SPβ,
202 but not against the closely related phage ϕ3T. It was recently found that ϕ3T encodes
203 an anti-defense protein, Gad1, that blocks Gabija activity, explaining this
204 difference[27,28]. However, here we observed that when overexpressed, Gabija does
205 confer potent protection from phage ϕ3T, indicating that Gabija defense overwhelms
206 phage anti-defense in this case.

207 To test our hypothesis more directly, we shifted our focus to a system for which we
208 can test the interaction between expression range and mechanisms of anti-defense
209 and evasion. It was recently discovered that a DSR2 system from *Bacillus subtilis*
210 provides defense by initiating NAD+ depletion upon recognition of a phage tail-tube
211 protein[29]. It was shown that phage SPR propagation is inhibited by DSR2 while the
212 closely related phage SPβ is not. Two features explain the failure of DSR2 to defend
213 against SPβ – first, the tail-tube protein of SPβ has lower affinity to DSR2. Second, SPβ
214 encodes for an anti-defense protein, Dsad1, which inhibits DSR2 through direct
215 competitive binding[29].

216 In the process of deciphering the mechanism of DSR2 defense, several SPR-SPβ phage
217 hybrids were made. We used two such hybrids for our purposes – one hybrid which
218 possesses the tail-tube protein of SPβ but does not code for Dsad1 (hybrid J76; an
219 'evading' hybrid), and another which possesses the tail-tube protein of SPR, but
220 additionally encodes for Dsad1 (hybrid J78; a 'neutralizing' hybrid) (Fig 2C). We tested
221 the efficiency with which SPR, SPβ, and these two hybrids could form plaques on a
222 lawn of bacteria expressing DSR2 at different levels (efficiency of plating, EOP).

223 As expected, under native expression, DSR2 could only defend against phage SPR. We
224 next cloned the *dsr2* gene under IPTG-induction and found that protection range
225 increased as we increased *dsr2* expression levels (Fig. 2C). First, we find that leaky
226 expression from the inducible *dsr2* system was already higher than that of the native
227 system and defended against the 'evading' hybrid even when no IPTG was added. At
228 a higher expression level (30 μM IPTG), DSR2 defended against the 'neutralizing'

229 hybrid as well, and finally at yet higher expression (100 µM IPTG), defense was
230 observed even against phage SPβ, which utilizes both strategies (Fig. 2C;
231 Supplementary Figure 7).

232 In total, these results show that the expansion of protection range with expression
233 level is widespread and that it may generally be explained by overcoming different
234 phage strategies of evasion and anti-defense.

235 **Sufficient increase of defense system expression leads to reduced growth**

236 An increased range of protection could potentially be highly beneficial to bacteria, and
237 increasing the strength of a promoter is a relatively simple evolutionary adaptation.
238 However, our results indicate that native expression levels of defense systems are far
239 from those maximizing protection range (Fig 1G, H; Fig. 2A, C). We reasoned that this
240 may potentially be explained by a substantial cost associated with increased
241 expression levels. To explore this, we first returned to *spbK* to test the expression-
242 dependent cost of this system (Fig. 3A, B). Using the IPTG-dependent, s*pbK*^{ind} strain,
243 we found that at high IPTG levels (>=50µM), that are beyond the range used to
244 examine protection (Fig. 1A-H), bacteria did not grow at all or exhibited substantially
245 delayed growth (Fig. 3A). Bacteria showed near normal growth at lower IPTG levels
246 (<=30µM) when examined in monoculture. To better identify smaller growth defects,
247 we used a coculture assay to compete differentially fluorescently labeled wild-type
248 strain and a strain encoding the inducible *spbK* at different IPTG levels (methods). We
249 find that *spbK*-expressing cells showed a sharp reduction in competitive fitness at
250 induction levels of 30µM (P=2*10^-4, two-tailed paired t-test; Fig. 3C).

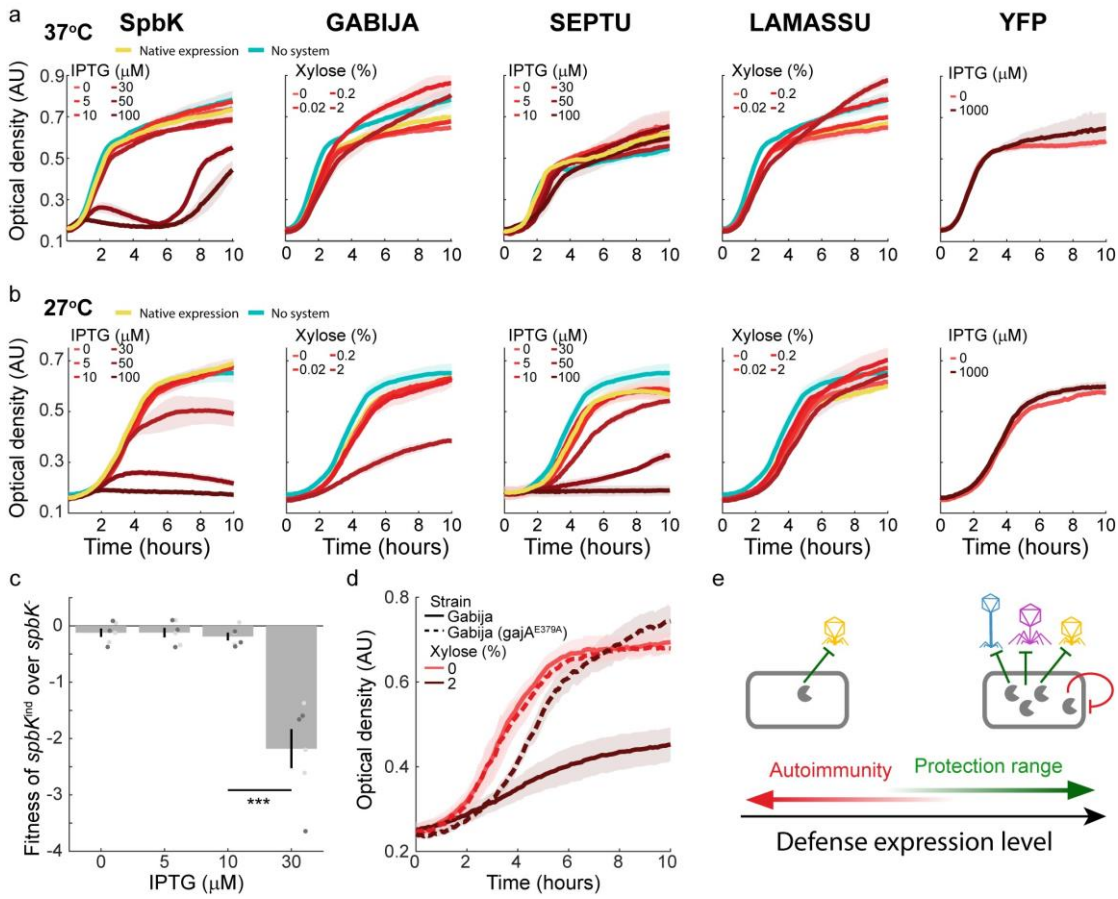

Figure 3: Defense overexpression leads to autoimmunity in multiple defense systems. (a, b) Growth curves of bacteria expressing defense systems or a yellow fluorescent protein (YFP) at different levels, at 37° (a) or 27° (b). Mean OD of n=3 biological replicates and and s.e.m. (lighter shade) are shown. (c) Fitness of *spbK*^{ind} over *spbK*$^{-}$ at different expression levels. Mean and s.e.m are shown. Individual points represent n=6 biological repeats. Light and dark points represent different fluorescent colors used (methods). * marks $p<0.05$. (d) Growth curves of strains expressing xylose induce Gabija (wild type sequence, solid lines) or a Gabija mutant (gajA^{E379A}; dashed lines) in the absence (light red) or presence (dark red) of xylose. Mean OD of n=3 biological replicates and and s.e.m. (lighter shade) are shown. (e) Illustration of the expression-controlled tradeoff between the benefit of protection range and the cost of autoimmunity. Green and red arrows represent opposing selection forces towards high or low expression, respectively.

We next asked whether other defense systems exhibit an expression-dependent cost as well. By tracking growth curves in monocultures at different expression levels, we found that Septu, but not Gabija and Lamassu showed an observable growth inhibition at high expression levels (Fig 3A). In addition to expression-level, other factors may also affect the activity and cost of defense systems. Previous reports have indicated that temperature may affect the activity of different defense systems[7,10]. We found that decreasing temperatures from 37° to 27° increased the cost of SPbK, Gabija and Septu overexpression (Fig 3B): growth inhibition by SPbK was observed at lower induction levels, and Gabija and Septu showed greater inhibition for the same induction levels. Lamassu did not incur an observable cost at either temperature (Fig.

3C). Other conditions or more sensitive assays may reveal other costs of different systems. Notably, it was found that a type II Lamassu system becomes costly to cells in the presence of some plasmids[30], suggesting that Lamassu systems may be costly under conditions other than those we tested.

Growth inhibition at high expression levels is due to autoimmunity

The cost associated with increased expression could result from the activity of defense systems, or from alternative sources such as metabolic burden. To test the possibility of cost due to metabolic burden, we first expressed a yellow fluorescent protein (YFP) under an IPTG-inducible promoter (Fig. 3A, B). We found that YFP expression had no observable effect on bacterial growth, even at saturating inducer levels (Figure S1B). For a more direct control and to further rule out other possible sources of cost, we introduced a point missense E379A mutation in the endonuclease domain protein of the Gabija system (*gajA*), which has previously been shown to abrogate defense[31]. We found that in contrast to the WT system, the overexpressed mutant Gabija did not impose an observable cost at 27° (Fig. 3D). This suggests that the cost of the system is a direct side-effect of its defensive function, which constitutes a form of autoimmunity.

In total, our results indicate that for diverse defense systems, increasing expression levels comes with a tradeoff – on the one hand a wider protection range is achieved by overcoming different phage strategies, but on the other hand the cost of autoimmunity increases as well (Fig 3E).

Discussion

Many studies have observed differences in protection range between different mechanisms. Here we show that increasing a systems expression can substantially alter its protection range – defense systems that under native expression afford a modest range of protection may hold the potential for a much broader protection range under increased expression levels. However, we show that for some systems increasing expression also comes with an increased cost, stemming from autoimmunity. This tradeoff may explain why native expression levels have not evolved to simply maximize protection range. We show that increased expression can increase protection range by circumventing different phage counter strategies against bacterial defense, including evasion and active disruption by anti-defense. Evidence to support this can also be found with the toxin-anti defense system ToxIN which successfully defends against phage T4 when carried on a multicopy plasmid, despite T4 carrying its own antitoxin[11]. In contrast, when integrated in a single copy in the bacterial chromosome, the defense-neutralizing antitoxin encoded by T4 is sufficient for defense.

The effectiveness of defense system overexpression against anti-defense mechanisms may come as a consequence of a basic asymmetry between bacteria and phages – while defense systems can be expressed prior to infection, expression of phage-encoded anti-defense mechanisms often begins only once infections

315 commence[7,11,27,32–34]. Indeed, anti-defense mechanisms such as anti-CRISPRs have
316 been shown to be expressed very highly and very early during infection, which may
317 assist phages to compensate for the initial disparity in favor of the pre-expressed
318 defense[26,35]. An alternative strategy to negate this asymmetry between defense and
319 anti-defense is by packaging anti-defense proteins into mature virions such that these
320 are injected into a host along with the phage genome[11,36].

321 Importantly, here we performed all experiments under a low MOI (0.1), but MOI may
322 be an additional variable affecting protection range. It has been shown that some anti-
323 CRISPRs are only effective at high MOIs[32,37]. This is the result of a cooperative effect in
324 which the culminative immunosuppressive effect of anti-CRISPRs expressed by phages
325 serially infecting single bacteria eventually leads to effective CRISPR inhibition and
326 phage propagation. A similar MOI-dependent effect is likely to occur in other anti-
327 defense mechanisms.

328 Several studies have previously examined the cost of defense systems, with varying
329 results. For instance, while the λ-phage-encoded RexAB system was reported to have
330 no observable cost in terms of growth rate or competition experiments[38], the anti-T4
331 Lit system was reported to incur a major cost when introduced on a high copy plasmid
332 into *E. coli* cells[39]. Restriction-modification systems have been observed to
333 occasionally cleave the bacterial chromosome, but this was only shown to be costly in
334 DNA-repair deficient mutants[40]. Additionally, it has been hypothesized that the
335 evolutionary pattern of frequent gain and loss of defense systems may be explained
336 by a major cost they incur[41–43]. Here we examined the cost of defense systems as a
337 function of expression level, showing that several divergent systems incur a major
338 expression dependent cost stemming from autoimmunity.

339 In contrast to other systems, Lamassu did not exhibit an observable cost on growth
340 rate even at high expression levels. As noted above, the cost of Lamassu may be more
341 pronounced in the presence of plasmids[30]. More generally, the cost of defense
342 systems may be condition-dependent. A striking example of condition-dependent cost
343 is that for all defense systems for which cost was observed, it was exasperated under
344 lower temperatures. It would be intriguing to pursue the source of this phenomenon
345 in future studies. More broadly, there are other potential aspects of the cost of
346 defense systems which we have not examined here. For instance, there could be an
347 infection-dependent cost of defense systems, as many systems target core cellular
348 processes upon activation[44–47], but not all phage infections are lethal. A prime example
349 is infection by temperate phages which could result in lysogeny.

350 The expression-controlled tradeoff between protection range and autoimmunity may
351 have several implications. Firstly, it suggests that regulation of expression is important
352 – high expression is very beneficial when infections are likely, but detrimental when
353 they are unlikely. It has been shown that the expression of some CRIPSPR systems is
354 controlled in a density-dependent manner, allowing for increased expression at high
355 bacterial densities when phages are more likely to spread throughout the
356 population[12–14]. Additionally, some systems have been reported to be induced upon

357 phage infection[48–53], though such late expression may fail to defend against rapidly
358 replicating phages. These may be seen as a possible solution to the tradeoff we
359 describe, and we envision that other forms of expression regulation may be revealed
360 in the future. A wholly different, but not mutually exclusive, solution to the tradeoff
361 we observed is possessing several defense systems, each specialized against a
362 different set of phages. This is also in agreement with some patterns of interactions
363 between phages and defense systems observed in natural populations[49,54]. An
364 assortment of multiple, lowly expressed, defense systems may achieve a broad
365 protection range, without the major cost associated with a single, highly expressed,
366 system. Therefore, the tradeoff we describe here may be a potential driver of the
367 frequent co-residence of multiple defense systems within the same genome[1], even
368 before considering possible synergistic interactions or layered activation of anti-phage
369 defense[42,49,55].

370

371 **Methods**

372 *Strain construction*

373 All bacterial strains, plasmids and primers used in this study are listed in
374 Supplementary Tables 1–3. To construct the new *B. subtilis* strains, standard
375 transformation protocols were used for genomic integration and plasmid
376 transformation[56]. All stains were constructed on the background of the PY79 *B.*
377 *subtilis* lab strain. An exception are strains harboring the Septu system, which were
378 constructed on the background of the *B. subtilis* BEST7003.

379 Defense systems used in this study consist of Gabija from *B. cereus* VD045, Lamassu
380 from Bacillus sp. NIO-1130, and Septu from *B. weihenstephanesis* KBAB4, all
381 discovered by Doron et al[2]. In addition, we used DSR2 from *B. subtilis* 29R (ref [29]) and
382 SpbK from *B. subtilis* strain 168. Sequences of all defense systems and native
383 promoters used are listed in Table 4.

384 *Growth media and conditions*

385 All experiments were performed in LB medium: 1% tryptone (Difco), 0.5% yeast
386 extract (Difco) and 0.5% NaCl. Liquid cultures were grown with shaking at 220 r.p.m
387 and a temperature of 37 °C. When preparing plates, medium was solidified by adding
388 2% agar. Antibiotics were added (when necessary) at the following concentrations:
389 spectinomycin, 100 μg ml^{-1}; chloramphenicol, 5 μg ml^{-1}; kanamycin, 10 μg ml^{-1};
390 macrolide, lincosamide and streptogramin, 3 μg ml^{-1};
391 erythromycin + 25 μg ml^{-1} lincomycin. For the experiments that involved infection,
392 MMB medium was used (LB supplemented with 0.1 mM of $MnCl_2$ and 5 mM of $MgCl_2$).

393 *Plaque forming assay*

394 Samples for PFU measurements were collected from cultures centrifuged for 5 min at
395 4,000 r.p.m. at room temperature. Next, the supernatant was filtered using a 0.2 µm
396 filter. Then, 100 µl of filtered supernatant at an appropriate dilution was mixed with
397 200 µl of the appropriate indicator strain grown to OD_{600} in MMB and left to incubate
398 at room temperature for 5 min. Three milliliters of molten LB-0.5% agar medium (at
399 60 °C) supplemented with 0.1 mM of $MnCl_2$ and 5 mM of $MgCl_2$ was added, mixed and
400 then quickly overlaid on LB-agar plates. Plates were then incubated at 37 °C for 1 h
401 and then overnight at room temperature to allow plaques to form.

402 *Infection experiments*

403 Strains were grown overnight in LB at 37° C with shaking at 220 r.p.m. then diluted by
404 a factor of 1:100 into fresh MMB medium supplemented with the indicated
405 concentration of inducers (either xylose or IPTG). On reaching OD_{600}= 0.3, cultures
406 were infected with phages at MOI = 0.1. To examine bacterial growth, OD
407 measurements at a wavelength of 600 nm were then performed in a 96-well plate
408 using a plate reader (VICTOR Nivo Multimode Plate Reader; PerkinElmer).
409 To measure phage propagation, strains were grown at 37° C with shaking at 220 r.p.m.
410 for 2 hrs subsequent to infection, at which point samples were collected for plaque
411 assays as described above. Plaque assays were performed on an indicator PY79 strain
412 that does not harbor defense systems.

413 *Isolation of ϕ29 escaper mutants*

414 *spbK*^{ind} were grown overnight in LB at 37° C with shaking at 220 r.p.m. then diluted by
415 a factor of 1:100 into fresh MMB medium supplemented with 30 µM of IPTG. Upon
416 reaching OD_{600}= 0.3, bacteria were infected with ϕ29 phages at MOI = 0.1. Lysates
417 were collected 2 hrs post infection and plaque assays were performed on *spbK*-
418 strains, as described above. Phages from 8 individual plaques were then used to infect
419 *spbK*^{ind} and *spbK*$^{-}$ strains, and bacterial growth curves were tracked as detailed above.
420 Gene *gp10* of all escaper mutants were then sequenced, as well as that of the ϕ29 wt
421 ancestor. Location and conservation score of the A139D mutated residue of Gp10
422 (PDB ID – 1JNB) was discerned using ConSurf[57].

423 *Co-expression with spbK*

424 Strains harboring *spbK* under control of wild type promoter and an additional xylose-
425 induced gene as indicated were grown to OD600= 0.3, and then diluted by a factor of
426 1:10 into fresh LB containing the indicated xylose concentration. Strains were then
427 placed in a plate reader and growth was tracked as described above.

428 *EOP on strains harboring DSR2*

429 Strains were grown ON in LB at 37° C with shaking at 220 r.p.m. then diluted by a factor
430 of 1:100 into fresh MMB medium supplemented with IPTG at the indicated

431 concentration. On reaching OD_{600}= 0.3, growing strains were used to perform plaque
432 assay with different phages, as detailed above.

433 *Defense systems cost experiments*

434 To examine bacterial growth during expression of defense systems, strains were
435 grown overnight in LB at 37° C with shaking at 220 r.p.m. then diluted by a factor of
436 1:100 into fresh LB medium. On reaching OD_{600}= 0.3, strains were diluted by a factor
437 of 1:10 into fresh LB medium supplemented with different concentrations of the
438 appropriate inducer (xylose or IPTG). and placed in the plate reader. OD
439 measurements at a wavelength of 600 nm were then performed as described above
440 at either 37° C or 27° C.

441 For competitions experiments, differentially fluorescent-marked strains were grown
442 to OD_{600}= 0.3, mixed at a 1:1 ratio. Co-cultures were then diluted at a factor of 1:10
443 and IPTG was added at the indicated concentration. After ON growth at 37° C with
444 shaking strain frequencies were measured using flow cytometry (Beckman Coulter
445 CytoFLEX flow cytometer). Relative fitness was calculated as the ratio of relative
446 frequency of the strains at the end of the experiment to their initial frequency.

447 *RT–qPCR measurements*

448 Strains grown ON were diluted by a factor of 1:100 into fresh LB medium containing
449 appropriate concentrations of IPTG. Upon reaching OD_{600}= 0.3 total RNA was
450 extracted from cells using a High Pure RNA Isolation Kit (Roche). Samples at different
451 time points were centrifuged for 5 min at 2,000 relative centrifugal force and pellets
452 were flash-frozen in liquid nitrogen. Then, 1 µg of RNA was reverse-transcribed to
453 complementary DNA (cDNA) using a qScript cDNA Synthesis Kit (Quanta BioSciences).
454 RT–qPCR was performed on a QuantStudio™ 1 System (Applied Biosystems) using
455 SYBR Green (Quanta BioSciences). The specificity of primers (listed in Supplementary
456 Table 3) was validated using a melt curve. The efficiency of the primers used was
457 between 95 and 105%, with calibration curves of r2 > 0.95. Thermocycling parameters
458 were as follows: holding stage at 95 °C for 1 min and 40 cycles of 2 steps—a first step
459 at 95 °C for 5 s and a second step at 60 °C for 30 s. Transcript levels were normalized
460 to levels of the reference gene *rpoB*. RNA samples were stored at −80 °C and cDNA
461 was stored at −20 °C. Nucleic acid quantification was performed by NanoDrop 2000c
462 Spectrophotometer (Thermo Fisher Scientific). Results were analysed using the
463 QuantStudio design & analysis software v1.5.2 by the standard ΔΔCt method.

464 **Acknowledgements**

465 We thank Shaul Pollak, and members of the Eldar lab for fruitful discussions and
466 comments on the manuscript. The Eldar lab is funded by a European Research Council

467 grant 724805 and by Israel Science Foundation grant 2228/21. Nitzan Aframian is
468 supported by the Israeli Academy of Science's Adams Fellowship.

469

470

471 **References**

472 1. Tesson, F. *et al.* Systematic and quantitative view of the antiviral arsenal of
473 prokaryotes. *Nat. Commun.* **13**, 2561 (2022).

474 2. Doron, S. *et al.* Systematic discovery of antiphage defense systems in the microbial
475 pangenome. *Science* **359**, eaar4120 (2018).

476 3. Bernheim, A. & Sorek, R. The pan-immune system of bacteria: antiviral defence as a
477 community resource. *Nat. Rev. Microbiol.* **18**, 113–119 (2020).

478 4. Ofir, G. *et al.* DISARM is a widespread bacterial defence system with broad anti-
479 phage activities. *Nat. Microbiol.* **3**, 90–98 (2018).

480 5. Adler, B. A. *et al.* RNA-targeting CRISPR-Cas13 Provides Broad-spectrum Phage
481 Immunity. 2022.03.25.485874 Preprint at https://doi.org/10.1101/2022.03.25.485874
482 (2022).

483 6. Gao, L. A. *et al.* Prokaryotic innate immunity through pattern recognition of
484 conserved viral proteins. *Science* **377**, eabm4096 (2022).

485 7. LeRoux, M. *et al.* The DarTG toxin-antitoxin system provides phage defence by ADP-
486 ribosylating viral DNA. *Nat. Microbiol.* **7**, 1028–1040 (2022).

487 8. Johnson, C. M., Harden, M. M. & Grossman, A. D. Interactions between mobile
488 genetic elements: An anti-phage gene in an integrative and conjugative element protects
489 host cells from predation by a temperate bacteriophage. *PLOS Genet.* **18**, e1010065 (2022).

490 9. Zhang, T. *et al.* Direct activation of a bacterial innate immune system by a viral
491 capsid protein. *Nature* **612**, 132–140 (2022).

492 10. Bobonis, J. *et al.* Bacterial retrons encode phage-defending tripartite toxin–antitoxin
493 systems. *Nature* **609**, 144–150 (2022).

494 11. Srikant, S., Guegler, C. K. & Laub, M. T. The evolution of a counter-defense
495 mechanism in a virus constrains its host range. *eLife* **11**, e79549 (2022).

496 12. Severin, G. B. *et al.* Activation of a Vibrio cholerae CBASS anti-phage system by
497 quorum sensing and folate depletion. *mBio* **0**, e00875-23 (2023).

498 13. Patterson, A. G. *et al.* Quorum Sensing Controls Adaptive Immunity through the
499 Regulation of Multiple CRISPR-Cas Systems. *Mol. Cell* **64**, 1102–1108 (2016).

500 14. Høyland-Kroghsbo, N. M. *et al.* Quorum sensing controls the *Pseudomonas*
501 *aeruginosa* CRISPR-Cas adaptive immune system. *Proc. Natl. Acad. Sci.* **114**, 131–135 (2017).

502 15. Weiner, M. P. & Zahler, S. A. Genome Homology and Host Range of Some SPβ-
503 related Bacteriophages of Bacillus Subtilis and Bacillus amyloliquefaciens. *J. Gen. Virol.* **69**,
504 1307–1315 (1988).

505 16. Kohm, K. & Hertel, R. The life cycle of SPβ and related phages. *Arch. Virol.* (2021)
506 doi:10.1007/s00705-021-05116-9.

507 17. Noyer-Weidner, M., Jentsch, S., Pawlek, B., Günthert, U. & Trautner, T. A. Restriction
508 and modification in Bacillus subtilis: DNA methylation potential of the related
509 bacteriophages Z, SPR, SP beta, phi 3T, and rho 11. *J. Virol.* **46**, 446–453 (1983).

510 18. Kohm, K. *et al.* Structural and functional characterization of MrpR, the master
511 repressor of the Bacillus subtilis prophage SPβ. *Nucleic Acids Res.* **51**, 9452–9474 (2023).

512 19. Brady, A. *et al.* The arbitrium system controls prophage induction. *Curr. Biol.* **31**,
513 5037-5045.e3 (2021).

514 20. Warner, F. D., Kitos, G. A., Romano, M. P. & Hemphill, H. E. Characterization of SPβ:
515 a temperate bacteriophage from Bacillus subtilis 168M. *Can. J. Microbiol.* **23**, 45–51 (1977).

516 21. Dedeo, C. L., Cingolani, G. & Teschke, C. M. Portal Protein: The Orchestrator of
517 Capsid Assembly for the dsDNA Tailed Bacteriophages and Herpesviruses. *Annu. Rev. Virol.* **6**,
518 141–160 (2019).

519 22. In vitro incorporation of the phage Phi29 connector complex - ScienceDirect.
520 https://www.sciencedirect.com/science/article/pii/S0042682209004942.

521 23. Simpson, A. A. *et al.* Structure determination of the head–tail connector of
522 bacteriophage ϕ29. *Acta Crystallogr. D Biol. Crystallogr.* **57**, 1260–1269 (2001).

523 24. Ben Chorin, A. *et al.* ConSurf-DB: An accessible repository for the evolutionary
524 conservation patterns of the majority of PDB proteins. *Protein Sci.* **29**, 258–267 (2020).

525 25. Stokar-Avihail, A. *et al.* Discovery of phage determinants that confer sensitivity to
526 bacterial immune systems. 2022.08.27.505566 Preprint at
527 https://doi.org/10.1101/2022.08.27.505566 (2022).

528 26. Samuel, B. & Burstein, D. A diverse repertoire of anti-defense systems is encoded in
529 the leading region of plasmids. 2023.02.15.528439 Preprint at
530 https://doi.org/10.1101/2023.02.15.528439 (2023).

531 27. Yirmiya, E. *et al.* Phages overcome bacterial immunity via diverse anti-defense
532 proteins. 2023.05.01.538930 Preprint at https://doi.org/10.1101/2023.05.01.538930 (2023).

533 28. Antine, S. P. *et al.* Structural basis of Gabija anti-phage defense and viral immune
534 evasion. 2023.05.01.538945 Preprint at https://doi.org/10.1101/2023.05.01.538945 (2023).

535 29. Garb, J. *et al.* Multiple phage resistance systems inhibit infection via SIR2-dependent
536 NAD+ depletion. *Nat. Microbiol.* **7**, 1849–1856 (2022).

537 30. Jaskólska, M., Adams, D. W. & Blokesch, M. Two defence systems eliminate plasmids
538 from seventh pandemic Vibrio cholerae. *Nature* **604**, 323–329 (2022).

539 31. Cheng, R. *et al.* A nucleotide-sensing endonuclease from the Gabija bacterial defense
540 system. *Nucleic Acids Res.* **49**, 5216–5229 (2021).

541 32. Borges, A. L. *et al.* Bacteriophage Cooperation Suppresses CRISPR-Cas3 and Cas9
542 Immunity. *Cell* **174**, 917-925.e10 (2018).

543 33. Benzer, S. Fine structure of a genetic region in bacteriophage. *Proc. Natl. Acad. Sci.*
544 **41**, 344–354 (1955).

545 34. Koonin, E. V. & Makarova, K. S. Anti-CRISPRs on the march. *Science* **362**, 156–157
546 (2018).

547 35. Stanley, S. Y. *et al.* Anti-CRISPR-Associated Proteins Are Crucial Repressors of Anti-
548 CRISPR Transcription. *Cell* **178**, 1452-1464.e13 (2019).

549 36. Bair, C. L., Rifat, D. & Black, L. W. Exclusion of Glucosyl-Hydroxymethylcytosine DNA
550 Containing Bacteriophages Is Overcome by the Injected Protein Inhibitor IPI*. *J. Mol. Biol.*
551 **366**, 779–789 (2007).

552 37. Landsberger, M. *et al.* Anti-CRISPR Phages Cooperate to Overcome CRISPR-Cas
553 Immunity. *Cell* **174**, 908-916.e12 (2018).

554 38. Refardt, D., Bergmiller, T. & Kümmerli, R. Altruism can evolve when relatedness is
555 low: evidence from bacteria committing suicide upon phage infection. *Proc. R. Soc. B Biol.*
556 *Sci.* **280**, 20123035 (2013).

557 39. Berngruber, T. W., Lion, S. & Gandon, S. Evolution of suicide as a defence strategy
558 against pathogens in a spatially structured environment. *Ecol. Lett.* **16**, 446–453 (2013).

559 40. Pleška, M. *et al.* Bacterial Autoimmunity Due to a Restriction-Modification System.
560 *Curr. Biol.* **26**, 404–409 (2016).

561 41. Bernheim, A. & Sorek, R. The pan-immune system of bacteria: antiviral defence as a
562 community resource. *Nat. Rev. Microbiol.* **18**, 113–119 (2020).

563 42. Iranzo, J., Lobkovsky, A. E., Wolf, Y. I. & Koonin, E. V. Immunity, suicide or both?
564 Ecological determinants for the combined evolution of anti-pathogen defense systems. *BMC*
565 *Evol. Biol.* **15**, 43 (2015).

566 43. Koonin, E. V., Makarova, K. S., Wolf, Y. I. & Krupovic, M. Evolutionary entanglement
567 of mobile genetic elements and host defence systems: guns for hire. *Nat. Rev. Genet.* **21**,
568 119–131 (2020).

569 44. Lopatina, A., Tal, N. & Sorek, R. Abortive Infection: Bacterial Suicide as an Antiviral
570 Immune Strategy. *Annu. Rev. Virol.* **7**, 371–384 (2020).

571 45. Aframian, N. & Eldar, A. Abortive infection antiphage defense systems: separating
572 mechanism and phenotype. *Trends Microbiol.* **31**, 1003–1012 (2023).

573 46. Rousset, F. & Sorek, R. The evolutionary success of regulated cell death in bacterial
574 immunity. *Curr. Opin. Microbiol.* **74**, 102312 (2023).

575 47. van Houte, S., Buckling, A. & Westra, E. R. Evolutionary Ecology of Prokaryotic
576 Immune Mechanisms. *Microbiol. Mol. Biol. Rev.* **80**, 745–763 (2016).

577 48. Quax, T. E. F. *et al.* Massive Activation of Archaeal Defense Genes during Viral
578 Infection. *J. Virol.* **87**, 8419–8428 (2013).

579 49. DeLong, J. P. *et al.* Towards an integrative view of virus phenotypes. *Nat. Rev.*
580 *Microbiol.* **20**, 83–94 (2022).

581 50. Agari, Y. *et al.* Transcription Profile of Thermus thermophilus CRISPR Systems after
582 Phage Infection. *J. Mol. Biol.* **395**, 270–281 (2010).

583 51. Fusco, S. *et al.* Transcriptome analysis of *Sulfolobus solfataricus* infected with two
584 related fuselloviruses reveals novel insights into the regulation of CRISPR-Cas system.
585 *Biochimie* **118**, 322–332 (2015).

586 52. Workman, R. E. *et al.* Anti-CRISPR proteins trigger a burst of CRISPR-Cas9 expression
587 that enhances phage defense. 2023.10.22.562561 Preprint at
588 https://doi.org/10.1101/2023.10.22.562561 (2023).

589 53. Westra, E. R. *et al.* Parasite Exposure Drives Selective Evolution of Constitutive
590 versus Inducible Defense. *Curr. Biol.* **25**, 1043–1049 (2015).

591 54. Hussain, F. A. *et al.* Rapid evolutionary turnover of mobile genetic elements drives
592 bacterial resistance to phages. *Science* **374**, 488–492 (2021).

593 55. Wu, Y. *et al.* Synergistic anti-phage activity of bacterial defence systems.
594 2022.08.21.504612 Preprint at https://doi.org/10.1101/2022.08.21.504612 (2023).

595 56. Harwood, C. R. Molecular biological methods for Bacillus. *No Title*.

596 57. Ashkenazy, H. *et al.* ConSurf 2016: an improved methodology to estimate and
597 visualize evolutionary conservation in macromolecules. *Nucleic Acids Res.* **44**, W344–W350
598 (2016).

599

600

601 **Supplementary figures**

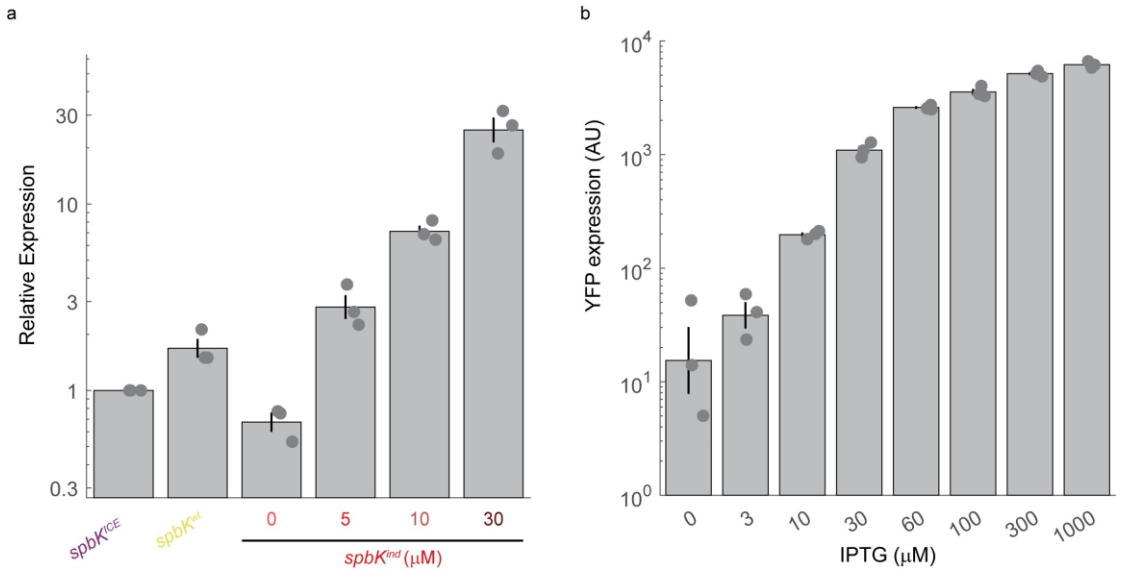

602

603 Supplementary Figure 1: native and induced *spbK* relative expression levels. (a) Relative
604 transcript levels of *spbK* in under different conditions, measured by RT-qPCR (methods).
605 *spbK*^{ICE} is a strain harboring the full ICE*bs*1 element, and *spbK*^{wt} a strain harboring *spbK* alone
606 under its native promoter. Shown are means and error bars represent s.e.m. Points represents
607 n=3 biological repeats. (b) YFP expression under an IPTG-inducible promoter at different
608 concentrations of IPTG. Shown are geometric means and s.e.m of the log. Individual points
609 represent n=3 biological repeats.

610

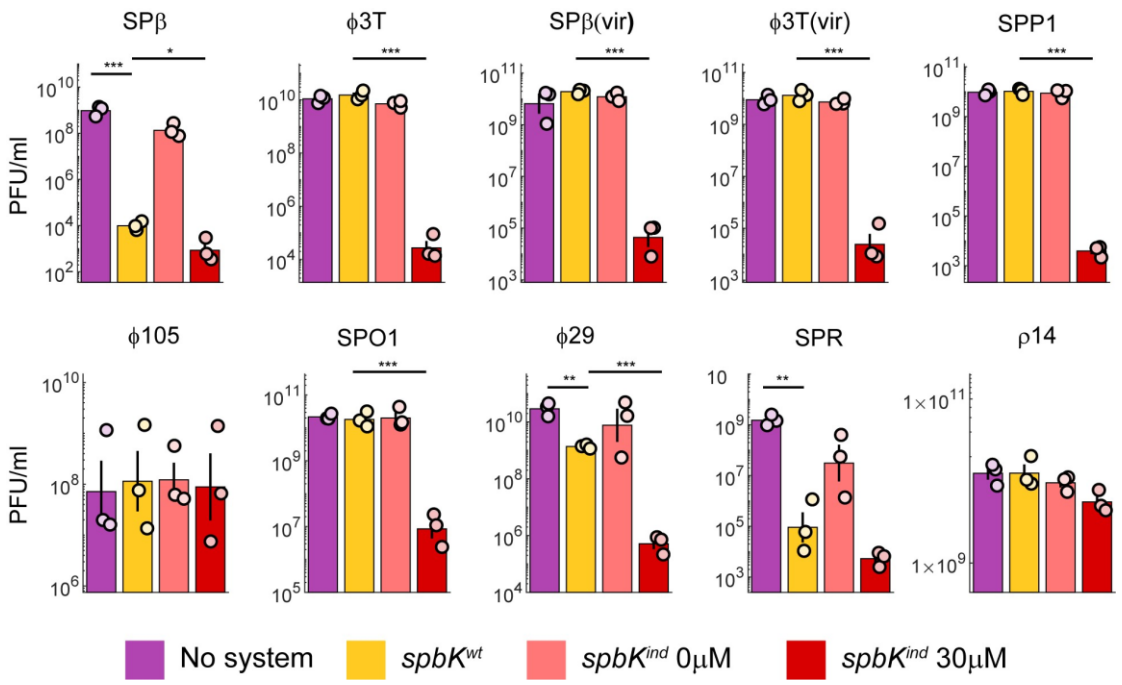

Supplementary Figure 2: PFU/ml of different phages 2 hrs post infection of strains harboring spbK at different expression levels. Shown are geometric means and s.e.m of the log. Individual points represent n=3 biological repeats. * marks p<0.05, ** marks p<0.005, and *** marks p<0.0005.

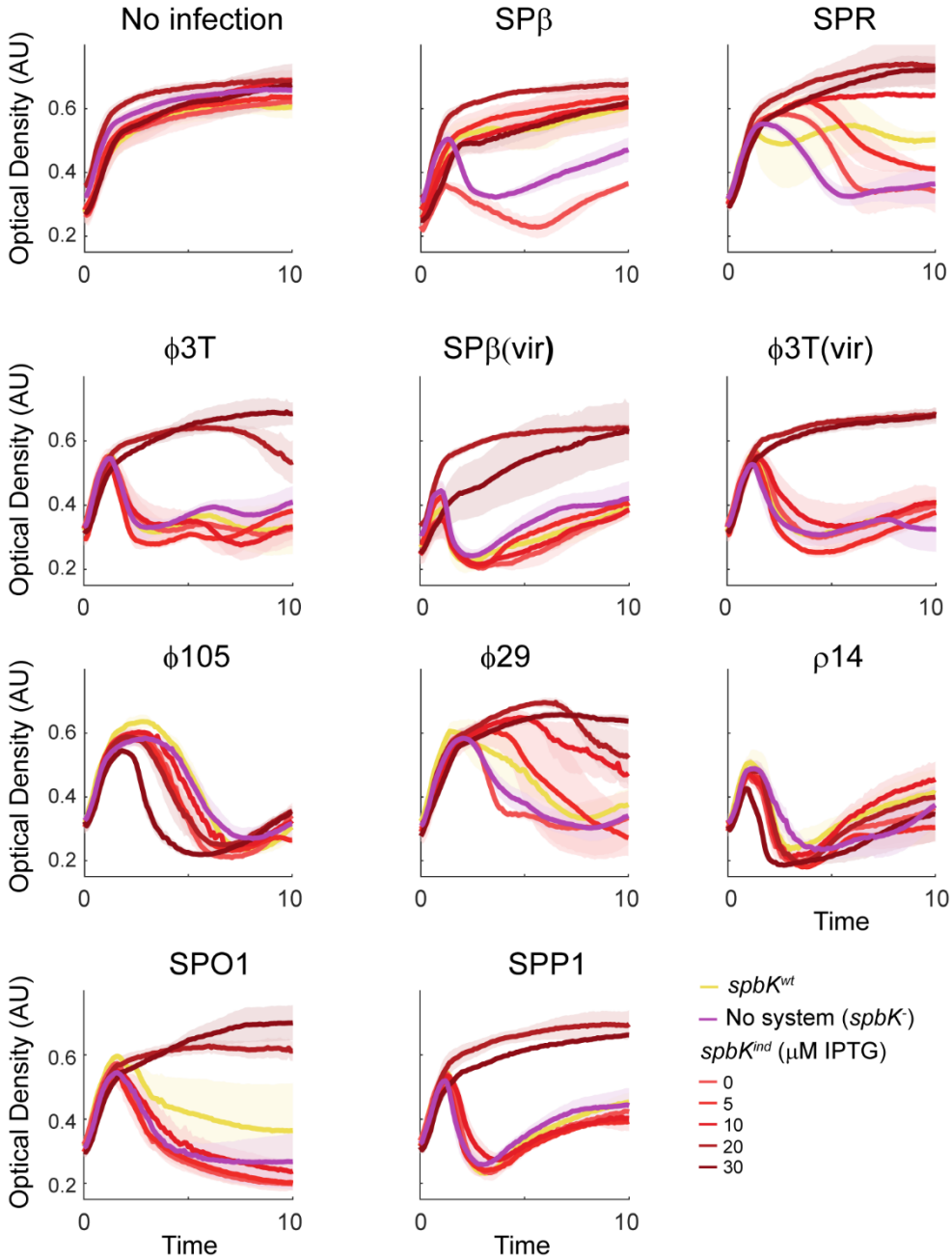

616

617 Supplementary Figure 3: Growth curves of bacterial strains expressing *spbK* at different
618 expression levels, infected by different phages. Mean OD of n=3 biological repeats and s.e.m
619 (lighter shade) are shown.

620

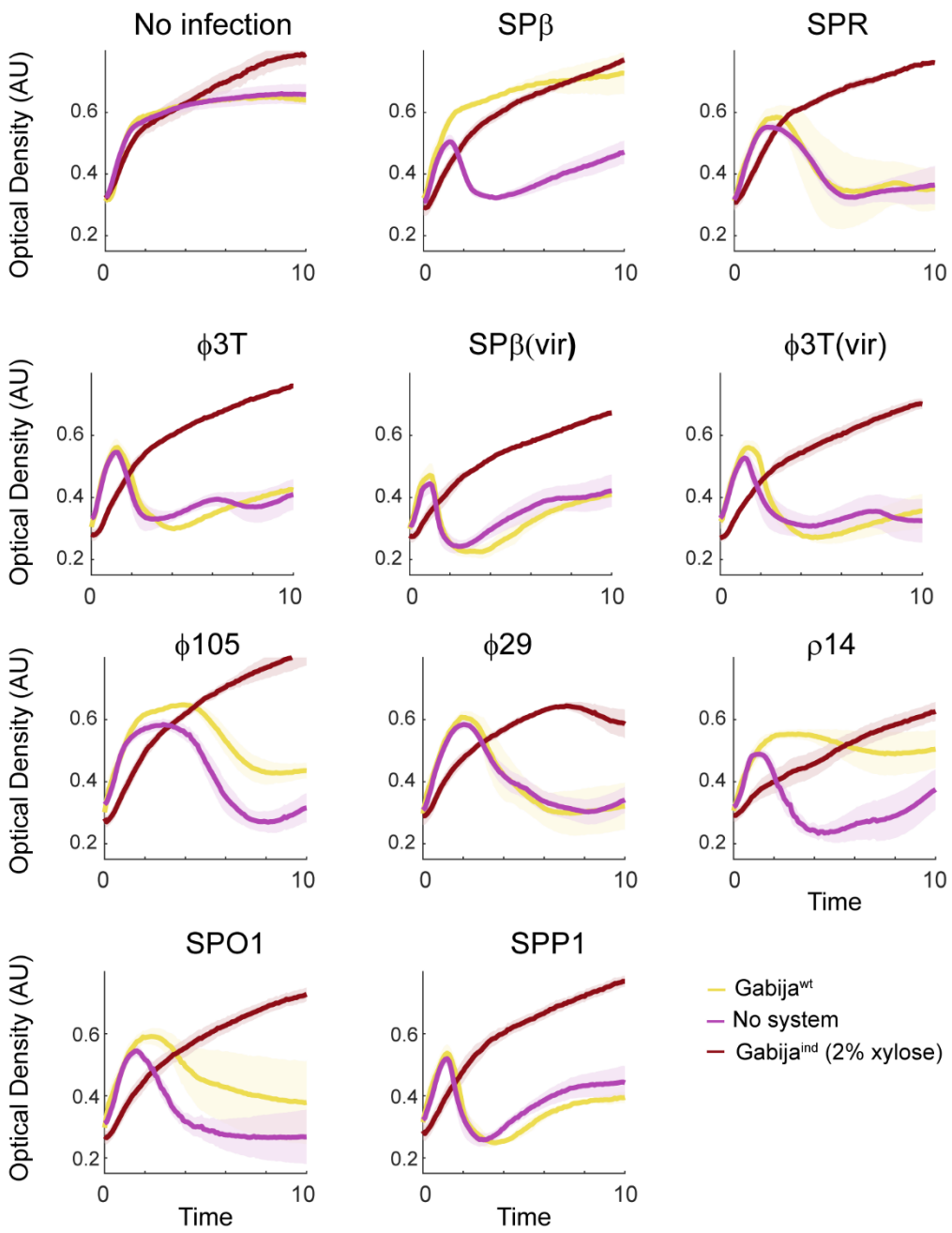

Supplementary Figure 4: Growth curves of bacterial strains expressing Gabija at different expression levels, infected by different phages. Mean OD of n=3 biological repeats and s.e.m (lighter shade) are shown.

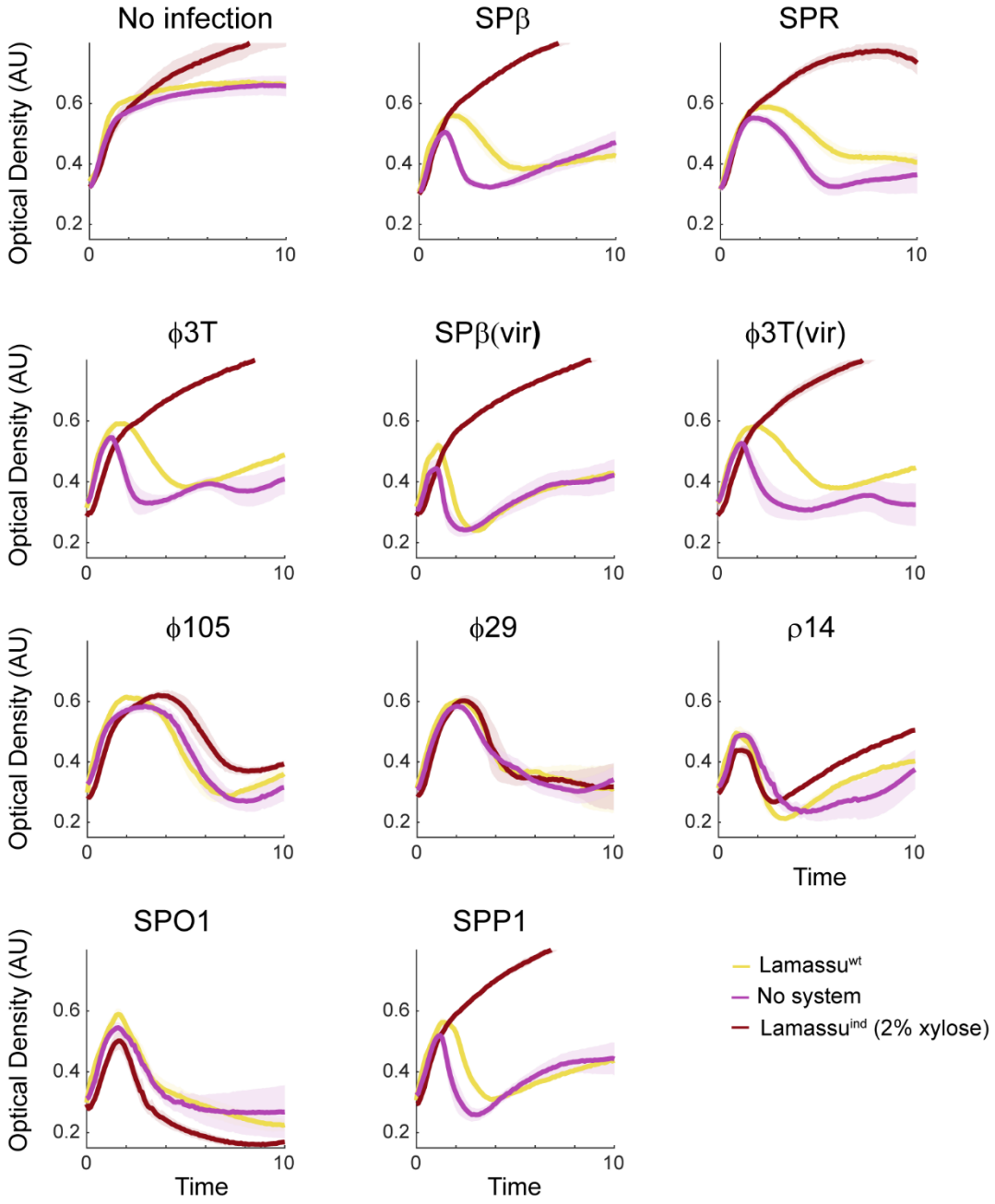

Supplementary Figure 5: Growth curves of bacterial strains expressing Lamassu at different expression levels, infected by different phages. Mean OD of n=3 biological repeats and s.e.m (lighter shade) are shown.

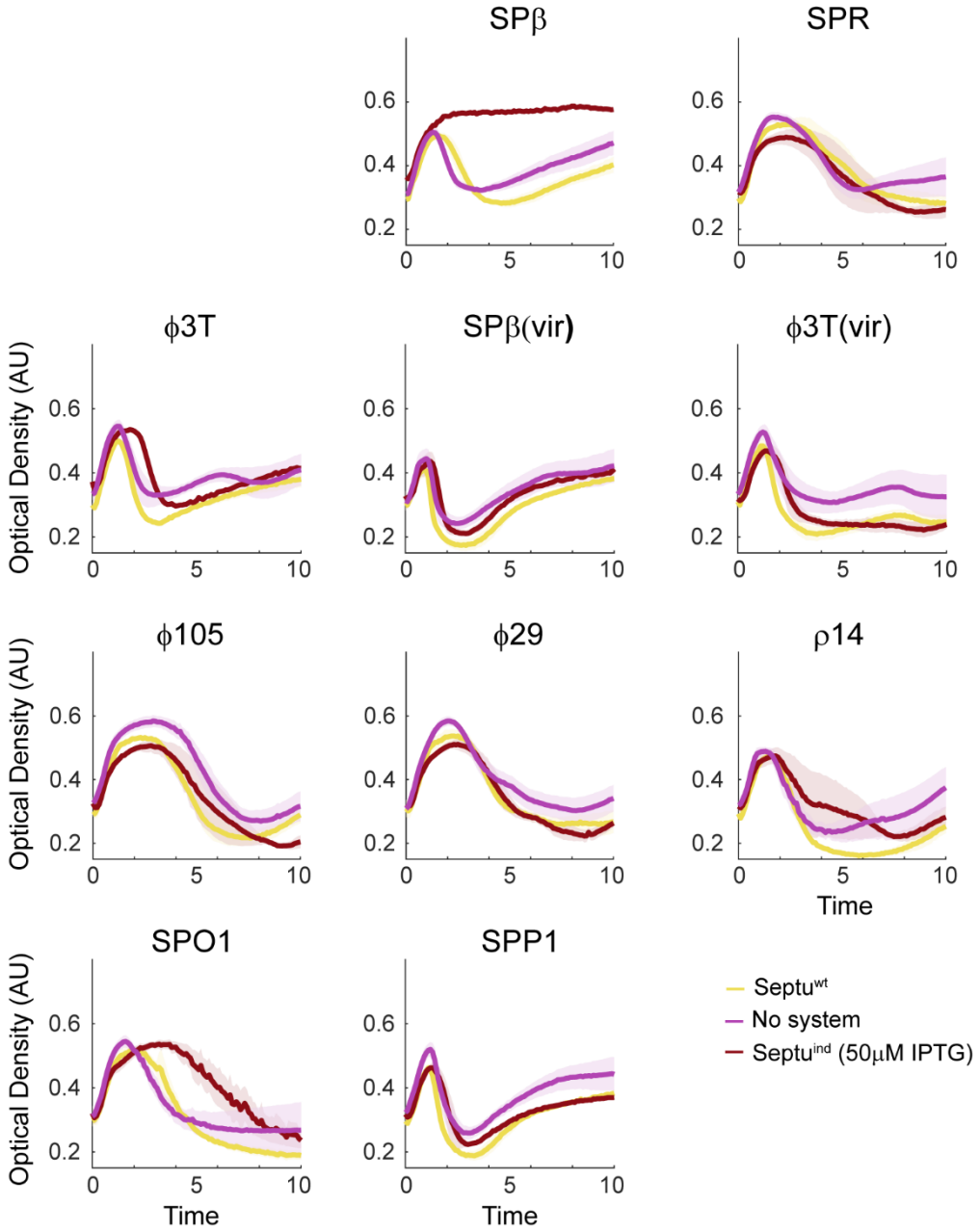

633

634 Supplementary Figure 6: Growth curves of bacterial strains expressing Septu at different
635 expression levels, infected by different phages. Mean OD of n=3 biological repeats and s.e.m
636 (lighter shade) are shown.

637

638

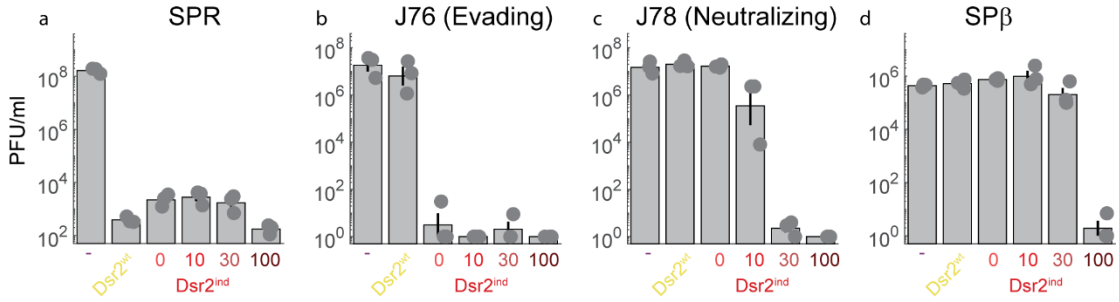

639

640 Supplementary Figure 7: PFU/ml of EOP assays of different phages infecting strains expressing
641 *dsr2* at different levels. Shown are geometric means and s.e.m of the log. Individual points
642 represent n=3 biological repeats.

643

644

645